ATMOSPHERIC ENVIRONMENT: X 14 (2022) 100172

Contents lists available at ScienceDirect

Atmospheric Environment: X

journal homepage: www.journals.elsevier.com/atmospheric-environment-x

Atmospheric dispersion simulation of an accidental smoke plume using a heat diffusion algorithm into a LES-STO coupled model

Cesar Aguirre [a,c,*], Guillermo Berri [b,c], Mariana Dezzutti [b], Juan Martin Queirel [b], Eliana Marcos [b], Carlos Sedano [a], Guillermo Rondán [a,c]

[a] Grupo Cli.M.A. - Facultad de Ciencias Agropecuarias, Universidad Nacional de Entre Ríos, Ruta 11, Km 10.5, E3100XAD, Oro Verde, Entre Ríos, Argentina
[b] Facultad de Ciencias Astronómicas y Geofísicas, Universidad Nacional de La Plata, Paseo del Bosque s/n, B1900FWA, La Plata, Buenos Aires, Argentina
[c] Consejo Nacional de Investigaciones Científicas y Técnicas, CONICET, Argentina

ARTICLE INFO

Keywords:
Fire
Smoke
Simulation
Stochastic
Satellite image

ABSTRACT

A high resolution earth satellite image with the visible smoke plume of a huge fire in the city of La Plata, Argentina, is used to verify the simulated plume with the fluid particle dispersion model LES-STO (large-eddy simulation - lagrangian stochastic one particle model). The initial and boundary conditions are provided by a boundary layer model forecast, and local meteorological observations validate the wind and temperature forecast with good results. The smoke plume is modeled by the continuous emission of fluid particles, initiated 4 h before the time of the satellite image in order to allow the model spin-up. Due to the lack of technical information about the fire, the emission parameters required by the model are estimated considering the dimensions of the burnt area and the products stored there. The spatial orientation and horizontal lateral extension of the modeled plume coincide with the smoke plume clearly visible in the satellite image. The conclusion of the study is that it is possible to use LES-STO with initial and boundary conditions provided by operational meteorological forecasts to make a diagnosis of those areas that could be affected by accidental emissions.

1. Introduction

The city of La Plata, located 56 km to the southeast of the city of Buenos Aires (Fig. 1), is the fourth most populated city of Argentina and the main political, administrative and educational center of the province of Buenos Aires. The city covers an area of 158.9 km^2, and the urban conglomerate that includes the neighboring cities of Berisso and Ensenada reaches a population of 1 million inhabitants.

On March 19, 2018 at about 1700 LST (local standard time), a huge fire started in the Mafissa plant, the most important synthetic fiber factory of the city of La Plata. The fire lasted 24 h and destroyed the facilities, despite the efforts of firefighters and Civil Defense authorities. When the fire started, the 96 workers on duties were able to evacuate the plant without injuries (Perfil, 2018). The huge plume of dense black smoke (Fig. 2) traveled several kilometers affecting different areas of the city, and the magnitude and duration of the event caused great concern for the population. Local authorities advised residents of the area to stay in their homes with doors and windows closed to prevent exposition to volatile particulate material. Despite the measures adopted by local authorities, repeatedly announced by the media, no air quality measurements were reported so such information, unfortunately, is not available.

Events like this one can be studied from the point of view of the atmospheric dispersion of smoke plumes caused by accidental and uncontrolled fires that often cause a major impact on population and properties. For example, Jenkins et al. (2001) has used coupled fire atmosphere models for numerical simulations, Berbery et al. (2008) used the WRF-ARW regional model outputs to study the predictability of the smoke episode that affected the city of Buenos Aires and its suburbs in April 2008 due to extensive pasture burning in the La Plata River delta, few tens of kilometers to the northwest of the city of Buenos Aires. Blanco and Berri (2013) simulated the smoke plume dispersion of that event using the Eta model forecast of the National Meteorological Service of Argentina and a coupled lagrangian trajectory dispersion model. Both studies concluded that the availability of operational forecasts could be useful for assisting local authorities in decision-making aimed at mitigating the harmful effects of such uncontrolled events on population and properties. Achtemeier et al. (2011) propose a *Daysmoke*

* Corresponding author. Ruta 11, Km 10.5, E3100XAD, Oro Verde, Entre Ríos, Argentina.
E-mail address: cesar.aguirre@fca.uner.edu.ar.com (C. Aguirre).

https://doi.org/10.1016/j.aeaoa.2022.100172
Received 30 December 2021; Received in revised form 7 April 2022; Accepted 13 April 2022
Available online 18 April 2022

Fig. 1. Location of the city of La Plata (red dot) in the La Plata River region of South America. The white rectangle depicts the area of the simulation, and the lower right box the location of the region in South America. (For interpretation of the references to color in this figure legend, the reader is referred to the Web version of this article.)

Fig. 2. Black smoke plume originated by the fire, photographed in the late afternoon of March 19, 2018.

model, a plume rise model developed for the simulation of smoke plumes from prescribed burns with good results in the comparison with the Briggs formulation (Briggs, 1975), Liu et al. (2011) evaluate and improve the performance of *Daysmoke* model in simulating smoke plume rise of prescribed burning with a combined approach of field measurements, numerical modeling and dynamical and statistical analysis. More recently, Bilyaz et al. (2021) investigate the smoke transport in high-rise buildings through elevator shafts and stairwells by using the computational fluid dynamics *Fire-STORM* model, Egorova et al. (2022) study the impact of mesoscale factors by considering the effects of the flame geometry and terrain slope, Stubbs et al. (2021) using the optically accessible facility combining traditional and optical diagnostic techniques study the combustion of wildland fuels and Awad et al. (2021) performed numerical simulations of grassland fires in order to relate the moisture content threshold of propagation success to the wind speed and the fuel load.

The availability of a high-resolution earth satellite image of the following morning, when the La Plata city fire was still burning and in which the smoke plume is clearly seen, motivated the present study. A fluid particle dispersion model, coupled to a mesoscale boundary layer model, simulates the dispersion of the smoke plume, and the satellite image provides the evidence to validate the spatial smoke plume layout obtained with the model. Therefore, the objective of the study is to evaluate the model ability to simulate the dispersion of the smoke plume caused by the accidental fire, and validate the results with the satellite image.

The following sections provide a brief description of the local meteorological conditions during the smoke event; the models employed and the validation of the wind and temperature forecast with local meteorological observations; the comparison of the modeled plume layout with the smoke plume observed in the high-resolution satellite image; and finally, the discussion of results and the conclusions of the study.

2. Methodology and experiment design

2.1. Simulation model and satellite image

The smoke plume is simulated with the Advanced Regional Prediction System (ARPS) model coupled at lagrangian stochastic one particle model (STO), with initial and boundary conditions provided by the Boundary Layer Model (BLM) forecast. The satellite image used to validate the modeled plume spatial layout corresponds to the 10-m resolution visible channel of Sentinel-2 satellite that flew over the region at 1058 LST of March 20, 2018. Sentinel-2 is an earth satellite in heliosynchronous orbit that passes over each point of the planet every 5 days at the same local solar time. The coincidence of one of its orbits with the clear sky conditions in the morning of that day, provided a clear image of the area. Despite the fire was extinguishing at that time, the high-resolution satellite image still shows the smoke plume.

The original eulerian finite difference of a large-eddy simulation (LES) code is the Advanced Regional Prediction System (ARPS), a non-hydrostatic and fully compressible mesoscale model. ARPS has been developed by the Center for Analysis and Forecasting of Storms (CAPS) (Xue et al., 2000), of the Oklahoma University. The code has been adapted by Aguirre et al. (2006) for the simulation of fluid particles by coupling the stochastic one-particle trajectory model in order to validate it with concentration measurements of a passive gas obtained in a wind tunnel over flat ground (Fackrell and Robins, 1982), and in the presence of a gentle sloping hill (Gong, 1991). Based on the eulerian form, the LES technique is an important tool for the simulation of wind turbulence in the atmosphere because the technique allows a three-dimensional description of the wind field and its time evolution. The model numerically integrates the time-dependent equations of mass balance, momentum and energy of large scale turbulence. This model not only simulates the wind field but also has sub-models of heat exchange and water vapor flux, cloud formation and rainfall taking into consideration the orography and land cover as well as the initial conditions of the ground and the atmospheric boundary layer. The turbulence intensity of the fluid that transports the fluid particles is taken into account in the simulation of the trajectories. With this approach, it is not possible to obtain a fully description of all turbulent eddies, so that the LES technique is applied for resolving the large scales of turbulence. The small scales are modeled by a sub-grid eddy viscosity model proposed by Germano et al. (1991) and implemented in ARPS by Aguirre et al. (2006). On the other hand, the lagrangian form is proposed to simulate the fluid particles trajectories. In the coupled LES-STO model, the intensity of turbulence is taken into account in the lagrangian stochastic equation (Aguirre et al., 2006). Aguirre and Brizuela (2016) describe the theoretical framework for this coupled model and show the results of fluid and solid particles dispersion from chimneys. The dispersion of total reduced sulfur plumes emitted from a pulp mill plant was simulated with ARPS, forced by initial and boundary conditions provided by BLM, for a series of events (Orcellet et al. 2016), with satisfactory results.

The simulation of emission plumes with fluid particles using stochastic lagrangian models has the advantage of simulating sources much smaller than the dimensions of the LES grid cells, compared to the Eulerian simulation of the trajectory of passive scalars such as heat sources. Therefore, it is convenient to use this type of LES-STO one particle two-way coupled models for simulations such as those of the present work. Aguirre et al. (2006) use the LES-STO model to simulate the atmospheric dispersion from a point source of NO in an atmosphere of O_3 in which an exothermic reaction produces NO_2 and O_2, obtaining the concentrations of both components downstream of the emitted plume. Vinkovic et al. (2006) use this coupled model to simulate the dispersion of small water drops emanating from the cooling towers of chemical plants; Sedano et al. (2019, 2020) for the dispersion and drift of sprayed droplets in agricultural activities, and Aguirre et al. (2014b) for simulating the dispersion of solid copper particles emanating from the chimneys of a smelting factory in the province of Tucumán, Argentina.

The BLM model is based on a dry, hydrostatic boundary layer and includes the basic conservation equations of momentum, mass and heat, with a first-order turbulence closure. We refer the reader to Berri et al. (2010) for the details about the model formulation. In brief, BLM has been specifically developed for simulating the low-level circulation over coastal regions, and has been employed in different studies in the La Plata River region (Sraibman and Berri, 2009; Ratto et al., 2014; Berri and Bertossa, 2018; Berri and Dezzutti, 2020). In the present study, BLM is forced with the operational Eta model forecast of the National Meteorological Service of Argentina. The horizontal resolution of BLM is 0.05°, which corresponds to an average of 5 km, with 79 points in the x direction (354 km) and 58 points in the y direction (316 km). The vertical domain has 16 levels between the surface and the material top at 2000 m, distributed according to a log–linear spacing. The upper boundary condition is defined from the 850 hPa Eta wind and temperature forecast and the lower boundary condition is defined from the Eta surface temperature forecast. The horizontal Eta resolution of 0.33° is interpolated to the 0.05° BLM resolution with the Cressman (1959) method. The 3-hourly Eta outputs are interpolated to the 30-s time step of BLM by means of cubic spline functions. At the lateral boundaries, variables are allowed to change in order to provide a zero gradient across the boundaries. BLM provides the initial and boundary conditions of wind, temperature and pressure, while the humidity conditions are taken from the Eta forecast since BLM is a dry model.

2.1.1. Initial and boundary conditions of the model

The initial and boundary conditions of wind, pressure and temperature required to run LES-STO are taken from the BLM forecast. This is possible by interpolating the time sequence of BLM outputs using a time-dependent boundary condition strategy. LES-STO has the capability of forcing the lateral boundary solutions with external data sets using relaxation boundary conditions from the coarser spatial resolution grid of BLM to the higher spatial resolution grid of LES-STO. The relaxation boundary condition proposed by Davies (1983) is:

$$\frac{\partial(\overline{\rho}\varnothing)}{\partial t} = -K_b\overline{\rho}(\varnothing - \varnothing_e), \tag{1}$$

where $\overline{\rho}$ is the horizontal average air density, $\varnothing$ is a prognostic variable and $\varnothing_e$ is the corresponding external future data value interpolated from the coarse grid. The relaxation coefficient K_b is defined as:

$$K_b = \frac{K_{b0}}{1 + \left[2\frac{i-i_b}{n_b-1}\right]^2} \quad for \quad i - i_b \le n_b - 1 \tag{2}$$

$$K_b = 0.0 \quad for \quad i - i_b > n_b - 1 \tag{3}$$

where K_{b0} is the maximum relaxation coefficient at the boundary, n_b the width of the relaxation zone in terms of the number of grid points, i the grid index and i_b the index of boundary grid point. In the present case we adopt $n_b = 5$ grid cells near the lateral boundary and K_{b0} is defined as the inverse of the folding damping time scale in the boundary relaxation zone τ, i.e. $K_{b0} = {}^1/_\tau$ with $\tau = 300$ s. This relaxation procedure forces the model boundary solution towards the external value. This method proved appropriate in the study of Aguirre et al. (2014a) using LES-STO forced with BLM forecast.

2.1.2. Coupled LES-STO model of fluid particles dispersion

The LES model is used for obtaining a 3-D description of the wind field and its temporal evolution. The 5.2.12 version of ARPS (Xue et al., 2000) has been adopted as LES code to solve the continuity and momentum equations by grid filtering. The convolution spatial filter operation $G(\Delta xi)$ where $\int G(\Delta xi)dxi = 1$, is carried out to obtain the large scales of turbulent flow where Δxi is the size of grid elements of the spatial domain. The spatial coordinates are written as x_i (with $i = 1, 2, 3$) and refer to the x (west-east), y (south-north) and z (vertical) directions, respectively. This filtered operation applied to the wind velocity u_i gives the large-scale component:

$$u_i^{\oplus} = \int u_i G(\Delta x_i) dx_i. \tag{4}$$

A detailed description of the process can be found in Xue et al. (2000).

Although LES is able of describing the large vortices of the wind flow, the dispersion of solid particles or gases is determined by the sub-grid turbulence, which is beyond the LES capability, so that the STO model is used for simulating the smaller scales. This model obtains the turbulent kinetic energy information from the resolved large scales by LES according to the Kolmogorov's theory of energy cascade follow Gicquel et al. (2002) using the *Fokker-Plank* equation which were based on previous work by Pope (1983) and Haworth and Pope (1986). Therefore, the coupling between the LES resolved scales and the coefficients of the deterministic and random terms of the stochastic model is implemented, and the detailed description of the LES-STO coupling can be found in Aguirre and Brizuela (2016) and Sedano et al. (2019, 2020). The lagrangian motion of the fluid particles that make up the smoke plume of the fire are:

$$\begin{cases} dX_i = U_i dt, \\ dU_i = \gamma_i dt + du_i^{\oplus} + \alpha_{ij} u_j^{\ominus} dt + \sqrt{C_0 \varepsilon}\delta_{ij}\, d\eta_j, \end{cases} \tag{5}$$

where γ_i is the fluid particle vertical acceleration due to external forces, $u_j^{\ominus}$ is the velocity component of fluid particle due to small scale turbulence (unresolved by LES), α_{ij} is a tensor related to the statistical properties of sub-grid turbulence in s^{-1}, ε is the dissipation rate of turbulent kinetic energy, C_0 is the Kolmogorov constant and $d\eta_j$ is the increment of a vector-valued Wiener process with zero mean and variance dt (see Appendix A for details).

2.1.3. Smoke plume simulation model

The temperature at which the smoke is released is much higher than the air temperature. When the turbulent smoke plume is lifted by buoyancy forces due to the thermal effect of the fire, it is cooled by the entrainment of ambient air around the plume. Consequently, the temperature of the air around the smoke plume increases as it rises with the smoke plume, and the smoke begins to cool due to entrainment from the surrounding air. When the temperatures of the entrained air and the smoke balance, the smoke column stops rising.

2.1.3.1. Temperature of smoke plume. The correct simulation of the smoke plume dispersion requires taking into account the effects that the large temperature difference has on the dynamics of the dispersion process, basically in two ways. On one hand, the buoyancy force due to the large density difference between the fluid particles and the

surrounding air entrained by the column of smoke, increases the vertical velocity of particles and, on the other hand, the heat diffusion due to the high temperature of fluid particles increases the temperature of the surrounding air entrained by the turbulence generated by the plume. Therefore, the diffusion model considers three different temperatures, namely the temperature of fluid particles (smoke), the temperature of the surrounding air entrained by the rising smoke plume, and the air temperature of the LES grid cell, i.e. the ambient air temperature in which there is smoke.

The model calculates the fluid particle temperature (T_f) with a heat diffusion equation, as a function of the temperature of each fluid particle and the temperature of the surrounding air (T_s). Subsequently, the air temperature of the LES grid cell (T_a) containing the smoke plume is computed by weighing the relative contributions of T_a itself and the temperature of surrounding air T_s.

The buoyancy force due to the high temperature difference between the fluid particles and the surrounding air is:

$$F_B = (\rho_s - \rho_f)\, g\, V_f = \rho_f\, V_f\, \frac{\Delta U_3}{\Delta t}, \tag{6}$$

where ρ_s and ρ_f are the density of the air surrounding the fluid particle and the density of the fluid particle, respectively, V_f is the fluid particle volume, $\Delta U_3/\Delta t$ is the fluid particle vertical acceleration and g is the acceleration of gravity. Therefore, the increase of the fluid particle vertical velocity due to the thermal effect is:

$$\Delta U_3 = \left(\frac{T_f}{T_s} - 1\right) g\, \Delta t, \tag{7}$$

in which the air and smoke densities are expressed as a function of their temperatures using the equation of perfect gases.

The heat transfer between the fluid particles and the surrounding air depends on their respective temperatures T_f and T_s. These two temperatures participate in a unique heat diffusion equation controlling the process, so that they are calculated in alternate steps using a discrete solution of the heat diffusion equation. In a first step, T_f is calculated with the following ordinary differential equation (Hsu and Chen, 1991) as a function of the temperature difference T_s - T_f:

$$\frac{dT_f}{dt} = \frac{C_{dif}}{2\, t_t}\left(T_s - T_f\right), \tag{8}$$

where T_s is equal to its last calculated value, C_{dif} is the turbulent diffusion coefficient and t_t is a characteristic turbulence time, both discussed below. The discrete solution of equation (8) (see Appendix B for the details) is:

$$T_f^{(t+\Delta t)} = T_s^{(t)} + e^{-\frac{C_{dif}}{2\, t_t}\Delta t}\left(T_f^{(t)} - T_s^{(t)}\right), \tag{9}$$

where $T_f^{(t+\Delta t)}$ and $T_f^{(t)}$ are the fluid particle temperatures at $(t+\Delta t)$ and (t) time steps, respectively, calculated in a lagrangian framework, i.e. following the motion of fluid particles, and $T_s^{(t)}$ is the temperature of surrounding air entrained by the smoke plume at time step (t), calculated in a eulerian framework, i.e. in each LES grid cell. Pope (1985) proposes $C_{dif} = 2.00$, and Michelot (1996) finds that $C_{dif} = 2.25$, which we adopt, gives better results in lagrangian-type simulations in fluid particle dispersion models when relating the characteristic time of turbulent diffusion and the concentration variance downstream the source.

The characteristic turbulence time $t_t = k/\varepsilon$ is the time scale of turbulence decay, which is directly proportional to the turbulent kinetic energy k and inversely proportional to the viscous dissipation rate of turbulent kinetic energy $\varepsilon = dk/dt$. These variables are available in ARPS code (Xue et al., 2000), so that equation (9) can be solved.

On the other hand, the high temperature of fluid particles T_f, leads to the increase of the surrounding air temperature T_s, and the heat transfer is controlled by the following equation as a function of the temperature difference $T_f - T_s$:

$$\frac{dT_s}{dt} = \frac{C_{dif}}{2\, t_t}\left(T_f - T_s\right), \tag{10}$$

in which we now use the last calculated value of T_f with equation (9). The consequent heating of the surrounding air will be a function, in addition to the temperature of the fluid particles, of their concentration in each LES grid cell where there is smoke, so that the discrete solution of equation (10), following a similar process described in Appendix B, is:

$$T_s^{(t+\Delta t)} = \frac{\sum\left(V_f^{(t+\Delta t)}\, T_f^{(t+\Delta t)}\right)}{\sum V_f^{(t+\Delta t)}} + e^{-\frac{C_{dif}}{2\, t_t}\Delta t}\left(T_s^{(t)} - \frac{\sum\left(V_f^{(t)} T_f^{(t)}\right)}{\sum V_f^{(t)}}\right) \tag{11}$$

The summation symbol is computed in a eulerian framework, i.e. in each LES grid cell, and the contribution of fluid particles to the surrounding air temperature T_s is now in terms of the volume-weighted average temperature T_f of all fluid particles in the grid cell.

The air temperature of the LES grid cell in the next time step $T_a^{(t+\ominus t)}$, is calculated by volumetric weighting of the surrounding air temperature at the next time step $T_s^{(t+\Delta t)}$ and the air temperature $T_a^{(t)}$ at the present time step, if $V_a > \sum V_f^{(t)}$, as:

$$T_a^{(t+\Delta t)} = \frac{\sum\left(V_f^{(t+\Delta t)} T_s^{(t+\Delta t)}\right) + \left(V_a - \sum V_f^{(t)}\right) T_a^{(t)}}{V_a}, \tag{12}$$

where V_a is the volume of the LES grid cell. In this model, the surrounding air entrained by the smoke plume is included into the volume of the fluid particles simulating the smoke plume in the present and the next time step. When the whole volume of the LES grid cell is filled with fluid particles, i.e. $V_a = \sum V_f^{(t)}$, equation (12) becomes:

$$T_a^{(t+\Delta t)} = T_s^{(t+\Delta t)} \tag{13}$$

2.1.3.2. vol change of fluid particles. It must be noted that the volume of fluid particles changes with time due to the cooler surrounding air that is entrained by the rising smoke plume and added into the plume. The mass flux at a given vertical level in the smoke plume is almost entirely attributable to air entrained into the plume from lower elevations. In the case of bent-over plumes, the mass flux contributed by the fire source itself can be negligible in comparison (Heskestad, 2016). For a weak plume, the author proposes that the mass flow rate of entrained air in a cross section $\Delta m_{ent}/\Delta t$, can be written as:

$$\frac{\Delta m_{ent}}{\Delta t} = E\left(\frac{g\, \rho_a^2}{C_p T_a}\, \frac{\Delta Q_c}{\Delta t}\right)^{1/3} (z - z_0)^{5/3}, \tag{14}$$

where $E = 0.153$ is a non-dimensional constant according to measurements by Yih (1952) and Cetegen et al. (1984), $C_p = 1005\, J\, kg^{-1}\, K^{-1}$ is the specific heat of air at constant pressure, z_0 is the virtual origin (Morton et al., 1956; Morton, 1959), i.e. the point of a virtual source from which the plume above the flame appears, z is the vertical distance from the ground, $\Delta Q_c/\Delta t$ is the convective part of the total heat release rate $\Delta Q/\Delta t$ from the fire source in $kJ\, s^{-1}$, often assumed to be equal to the theoretical heat release rate of the complete combustion of the burning material as:

$$\frac{\Delta Q}{\Delta t} = \frac{\Delta m_f}{\Delta t}\, h_c \tag{15}$$

The mass burning rate $\Delta m_f/\Delta t$ is in $kg\, s^{-1}$ and h_c is the net heat of combustion in $kJ\, kg^{-1}$. This is the bulk heat of combustion minus the latent heat of evaporation required to keep the water present in the combustion product in vapor state (Lyon et al., 1998). Part of the heat generated by the combustion is radiated away in all directions, but for

large fires, according to (Beyler, 2002), the radiative fraction tends to decrease with increasing fire size while the convective fraction tends to increase. Achtemeier et al. (2011) proposes that both, the convective part and the radiative part of the total heat release, are equally distributed for large fires.

The virtual origin for pool fires (Heskestad, 1983, 2016) can be expressed as:

$$z_0 = -\frac{1}{2} D_0 + 0.0659 \left(\frac{\Delta Q_c}{\Delta t}\right)^{2/5}, \tag{16}$$

with D_0 the equivalent diameter of the ignition area in meters. The volume of entrained air for each fluid particle can be estimated from equation (14) as:

$$\Delta V_f^{(t)} = E\,\Delta t \left(\frac{g}{\rho_a C_p T_a^{(t_0)}} \frac{\Delta Q_c}{\Delta t} \frac{1}{np_z}\right)^{1/3} \left(z^{(t)} - z_0\right)^{5/3}, \tag{17}$$

where np_z is the number of fluid particles at the vertical distance over source given by $z^{(t)}$. In equation (17), $T_a^{(t_0)}$ is the air temperature at the initial time step (t_0) when the fluid particle is ejected from the source. The fluid particle volume changes with time, as indicated above, due to the entrainment of cooler surrounding air so that the particle volume at the following time step $(t+\Delta t)$ is computed as:

$$V_f^{(t+\Delta t)} = V_f^{(t)} + \Delta V_f^{(t)} \tag{18}$$

2.1.3.3. Fluid particle concentration in the smoke plume. The initial concentration of fluid particles in the smoke plume will decrease as the plume rises due to the entrainment of cooler surrounding air. If $C^{(t_0)}$ is the volumetric concentration of fluid particles at the initial time of ejection from the fire, the relative concentration of fluid particles $C_r^{(t+\Theta t)}$, i.e. the ratio of the concentration at time step $(t+\Delta t)$ to the concentration at the initial time step at the source, is defined as:

$$C_r^{(t+\Theta t)} = \frac{C^{(t+\Delta t)}}{C^{(t_0)}} = \frac{V_f^{(t_0)}}{V_f^{(t+\Delta t)}} \tag{19}$$

2.1.4. Initial condition of smoke plume model

In this type of accidental fires, most of the specific data necessary to define the initial conditions of the model are difficult to obtain, or are not available as in the present case. Tagliaferri et al. (2022) indicate that in such situations, the physical emission parameters of the source generally cannot be measured directly, but are essential for simulation and in particular for determining downstream concentrations. The necessary information was determined by analyzing the consequences of the event and the elements that caused the fire, as well as the characteristics of the main fuel material that burned. The temperature of the fluid particles at the initial time step (t_0), when they are ejected from the ignition area, is estimated as $T_f^{(t_0)} = 600\,K$. This decision takes into account the auto-ignition temperature of the material in the storage room of the Mafissa factory where the fire started, i.e. paper, plastics, textile synthetic fibers and acrylonitrile-butadiene-styrene. As the factory was dedicated to the production of yarns and synthetic fibers for the textile industry, the flames soon spread, making it difficult to extinguish. "It's a huge fire in one of the storage rooms, which is full of fabrics, rags, chemicals, wood and even alcohol," said a firefighter.

Since not all fluid particles have the same temperature, an initialization algorithm was implemented using a Gaussian distribution of the temperature profile in a plane transverse to the smoke plume axis near the flames, according to measurements obtained from McCaffrey (1979) and corrected by Zukoski et al. (1984). These authors obtained a maximum temperature increase in the plume axis of $250\,K \pm 25\,K$, that is, a maximum deviation of 10% from the mean temperature. We consider that adopting a standard deviation equal to half of the maximum deviation found by these authors is a reasonable assumption. Since our estimate of the mean temperature of the plume axis near the flames is $T_f^{(t_0)} = 600\,K$, the ambient temperature deviation assumed for the model is $\sigma_{T_f^{(t_0)}} = 0.05\,T_f^{(t_0)} = 30\,K$.

The initial temperature of the (ith) fluid particle is computed as:

$$T_{f(i)}^{(t_0)} = T_f^{(t_0)} + \sigma_{T_f^{(t_0)}} \chi_{(i)}^{(t_0)}, \tag{20}$$

in terms of the standard deviation of temperature $\sigma_{T_f^{(t0)}}$, and a continuous random variable $\chi_{(i)}^{(t_0)}$ defined at the initial time step (t_0) of the simulation (see Appendix A for details).

The mean vertical velocity of fluid particles at the plume axis due to the thermal effect, at $z\,(m)$ level, can be obtained following Heskestad (1984), as:

$$\overline{U_3} = 3.4 \left(\frac{g}{C_p\,\rho_a\,T_a}\right)^{1/3} \left(\frac{\Delta Q_c}{\Delta t}\right)^{1/3} (z - z_0)^{-1/3} \tag{21}$$

The mean vertical velocity of fluid particles at ground level is obtained by making $z = 0$ in equation (21):

$$\overline{U_3^{(t_0)}} = 3.4 \left(\frac{g}{C_p\,\rho_a^{(t_0)}\,T_a^{(t_0)}}\right)^{1/3} \left(\frac{\Delta Q_c}{\Delta t}\right)^{1/3} (-z_0)^{-1/3} \tag{22}$$

As discussed above, not all fluid particles have the same temperature, therefore they will not have the same vertical velocity. As with the definition of the initial temperature, a similar randomization algorithm is applied to define the fluid particles initial velocity. The initial vertical velocity $U_{3(i)}^{(t_0)}$ of the (ith) fluid particle is calculated as $U_{3(i)}^{(t_0)} = \overline{U_3^{(t_0)}} + \sigma_{U_3^{(t_0)}} \chi_{(i)}^{(t_0)}$, where $\sigma_{U_3^{(t_0)}} = 0.05\,\overline{U_3^{(t_0)}}$ is the vertical velocity standard deviation, and $\chi_{(i)}^{(t_0)}$ is the same random variable of equation (20).

The initial volume of fluid particles is defined as the ratio of the volume of the ignition domain to the number of particles ejected at each time step:

$$V_f^{(t_0)} = \frac{A\,h}{np}, \tag{23}$$

in which A is the ignition area, h is the height of the burning building structure and np is the number of fluid particles ejected at each time step with $\Delta t = 1\,s$ from the ignition area.

The initial condition of the surrounding air temperature $T_s^{(t_0)}$ is computed as:

$$T_s^{(t_0)} = \frac{\sum\left(V_f^{(t_0)}\,T_f^{(t_0)}\right)}{\sum V_f^{(t_0)}} + e^{-\frac{C_{diff}}{2}\Delta t} \left(T_a^{(t_0)} - \frac{\sum\left(V_f^{(t_0)}\,T_f^{(t_0)}\right)}{\sum V_f^{(t_0)}}\right), \tag{24}$$

where the $T_s^{(t)}$ value of the right-hand side of equation (24) has been replaced by $T_a^{(t_0)}$ assuming that in the lower part of the smoke plume, the entrained air is at ambient temperature $T_a^{(t_0)}$.

The smoke plume elevation obtained from the model is compared with the plume rise from the well-known Briggs algorithm (Briggs, 1975; 1984) and used by Golubnichiy and Nedelina (2015) for modeling of the atmospheric air pollution for urban air basins, which gives the height of the plume axis downstream of the source, and the results are discussed below in Section 4.

2.2. Smoke plume data and simulation design

To simulate the dispersion of the smoke plume, LES-STO was run in the same horizontal domain of BLM (see Fig. 1), in a grid of 387 × 282 points with 1-km horizontal resolution and 33 vertically spaced levels

Fig. 3. The area of the Mafissa factory before the fire in March 2018 (left) and after the fire in September 2018 (right). Courtesy of Maxar Technologies - Google Earth Pro. The affected area by the fire is approximately 14000 m^2.

Fig. 4. Location of the Mafissa factory (1), and the meteorological stations of the region Agro (2), LPA (3), AERO (4) and Sicardi (5). The dashed line rectangle depicts the area of the smoke plume simulation described in Section 4. Courtesy of Maxar Technologies - Google Earth Pro.

according to a hyperbolic tangent function. As mentioned in Section 2, BLM provides the initial and boundary conditions for LES-STO. BLM is initialized with Eta-SMN forecasts and starts at 0600 LST on March 20, 2018, but the simulation with LES-STO starts at 0700 LST to allow 1 h for the BLM spin-up. As the Sentinel-2 image is at 1058 LST of March 20, 2018, the 4-h LES-STO simulation allows eliminating possible mismatches among variables as a consequence of the initialization. The LES-STO boundary conditions are updated every 15 min with the BLM outputs and every 10 min LES-STO records the position of the fluid particles that represent the result of the transport and diffusion of the smoke plume.

The fire source was placed at the Mafissa factory location (34.984°S, 58.034°W) and the smoke plume is represented by the dispersion of the continuous emission of $np = 10$ fluid particles per second ejected from the area of the fire source. Although the storage room where the fire broke out measured 30 m x 60 m, the affected area was approximately 14,000 m^2 (see Fig. 3). As mentioned in Section 2.2.4, we adopt $T_f^{(t_0)} = 600\ K$ as the value of exit temperature of the fire gases according to Achtemeier et al. (2011).

The convective part of the total heat release $\Delta Q_c/_{\Delta t}$ is estimated, following Achtemeier et al. 2011, as 50% of the total heat release $\Delta Q/_{\Delta t}$, equation (15), so that $\Delta Q_c/_{\Delta t} = 4406.25\ kJ\ s^{-1}$. The mass burning rate $\Delta m_f/_{\Delta t}$ is estimated as $0.2315\ kg\ s^{-1}$, considering that the igneous material housed in the storage room burnt out completely in one day, i.e. $20,000\ kg$ of barrels containing acrylonitrile-butadiene-styrene, which is a highly flammable input in the textile industry. The net heat of combustion is defined as $h_c = 38,070\ kJ\ kg^{-1}$, following Lyon et al. (1998). Considering an ignition area of $X_a = 100\ m$, $Y_a = 140\ m$ (see Fig. 3), the equivalent diameter is $D_0 = \sqrt{\frac{4}{\pi}(X_a\ Y_a)} = 133.51\ m$, and the virtual origin in equation (16) is. $z_0 = -64.87\ m$.

Table 1
Daily average BLM absolute forecast error of temperature (°C), wind direction (deg.) and wind speed (ms^{-1}) at meteorological stations of La Plata (LPA), Sicardi (SI), Agronomía (Agro) and La Plata Aero (AERO).

average absolute error	LPA	SI	AGRO	AERO
temperature (°C)	2.4	2.3	2.3	2.5
wind direction (deg)	18	24	16	26
wind speed (ms^{-1})	1.7	1.4	1.3	1.2

The initial vertical velocity of fluid particles is calculated with equation (22), as a function of the temperature and density of the air, which, as discussed above, varied during the simulation period. With $T_a^{(t_0)} = 292\ K$ and $\rho_a^{(t_0)} = 1.2088\ Kg\ m^{-3}$ in equation (22), the mean value of fluid particles initial vertical velocity is $\overline{U_3^{(t_0)}} = 4.18\ m\ s^{-1}$.

The position of the fluid particles at each time step allows calculating the mean relative concentration of particles contained in 3-D boxes of 50 m side, downstream of the smoke plume, according to equation (19).

3. Meteorological model validation

The fire event lasted from the afternoon of March 19, 2018 until the afternoon of March 20, 2018, during which there were no significant weather conditions over the region, partly cloudy sky the first day and clear sky the following day.

Since the position of the smoke plume obtained with the model is compared with the Sentinel-2 satellite image of 1058 LST of March 20, 2018, BLM predictions are validated with the observations of four meteorological stations of the region during that day (see Fig. 4 for location).

Table 1 summarizes the daily averaged BLM absolute error (between 0700 and 2100 LST), defined as the absolute value of the difference between forecast and observation, and Fig. 5 compares hourly BLM forecasts and observations.

The average temperature errors are between 2.3°C and 2.5°C, and the daily temperature cycle of 10°C is quite similar in all the stations, slightly underestimated in the morning and overestimated in the afternoon. The average error in wind direction ranges between 16° at AGRO and 26° at AERO, and the model forecast reproduces reasonably well the observed 130-degree wind shift from NW to S during the day. Regarding wind speed, the average error ranges between $1.2\ m\ s^{-1}$ at AERO and $1.7\ m\ s^{-1}$ at LPA, although the model does not reproduce the observed short-term wind speed oscillations. We consider that, in general, the model forecast represents reasonably well the observed meteorological conditions so that the BLM outputs provide reliable data for the plume simulation.

4. Results and discussion

Fig. 6 presents an hourly sequence from 0800 LST to 1300 LST of the modeled smoke plume spatial layout. As noted above, the fluid particles emission begins at 0700 LST, 1 h after the start of LES-STO modeling to allow for the model spin-up. The relative concentration of smoke is defined as the ratio of the concentration in each box to the concentration at the source, at each time step. The spatial layout of the smoke plume shown in Fig. 6 is obtained by computing the average of relative concentration of fluid particles contained in 3-D boxes of 50m side. The color scale expresses the relative concentration of fluid particles contained in all boxes between the surface and $1,200\ m$, which is the maximum height reached by the particles. This representation is considered appropriate for comparison as the satellite image represents

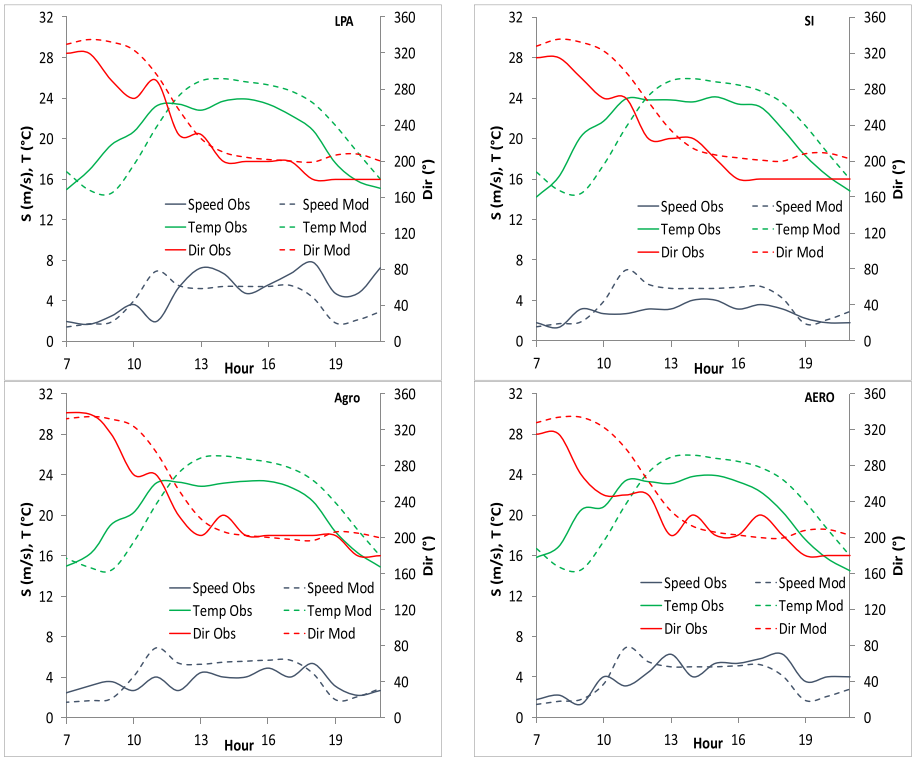

Fig. 5. Comparison of BLM forecasts of wind direction (red), wind speed (black) and temperature (green); and observations at La Plata (LPA), Sicardi (SI), Agronomía (Agro) and La Plata Aero (AERO) meteorological stations. Dashed lines correspond to BLM and full lines to observations. (For interpretation of the references to color in this figure legend, the reader is referred to the Web version of this article.)

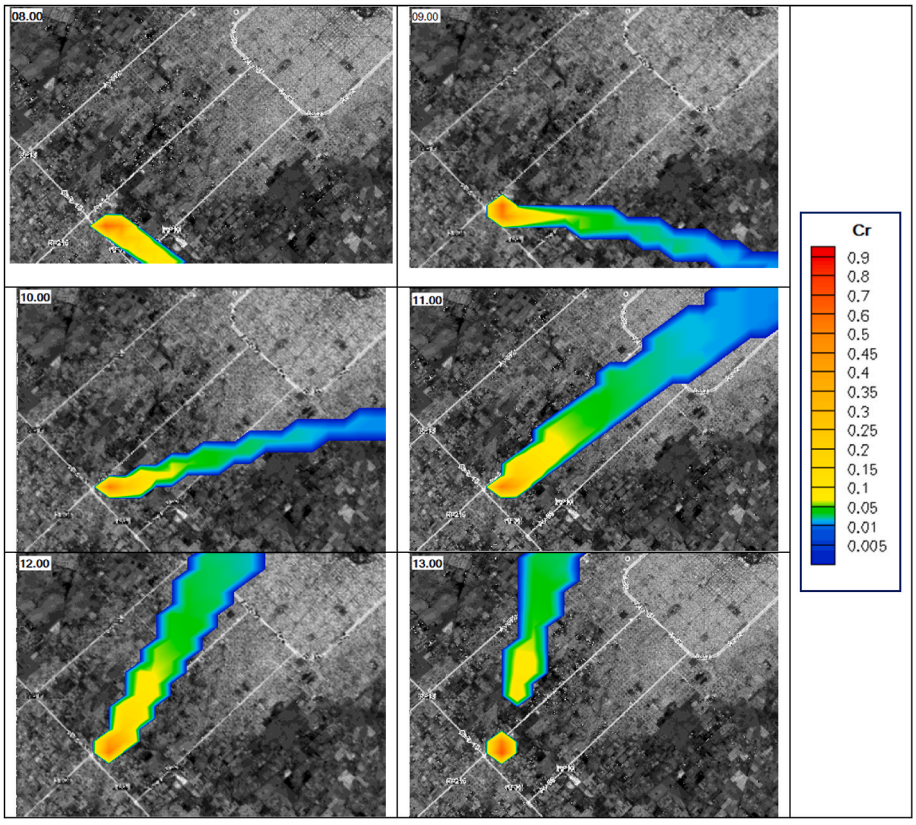

Fig. 6. Hourly sequence from 0800 LST to 1300 LST of the modeled smoke plume over the region delimited by the inner rectangle of Fig. 4. The color scale represents the relative concentration of smoke to the source fire computed in all 50-m side 3-D boxes between the surface and 1200 m. (For interpretation of the references to color in this figure legend, the reader is referred to the Web version of this article.)

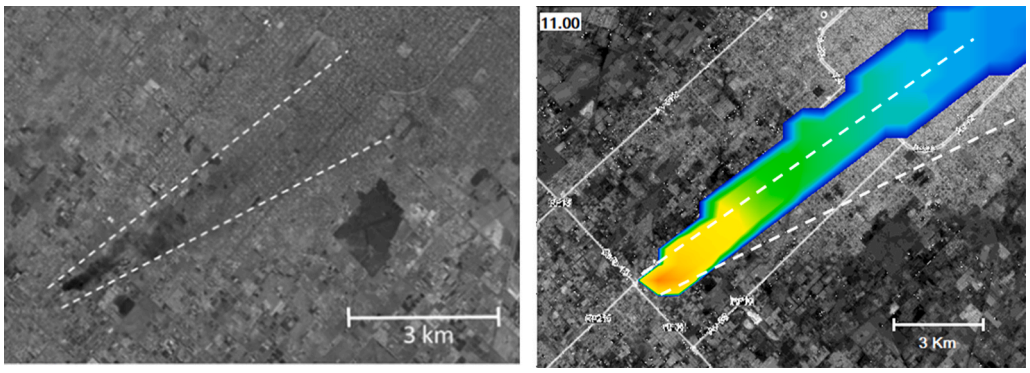

Fig. 7. Sentinel-2 image of March 20, 2018 at 1058 LST, with dashed lines delineating the smoke plume limits (left panel). Modeled smoke plume at 1100 LST (right panel) where the dashed lines represent the same smoke plume boundaries drawn in the left panel.

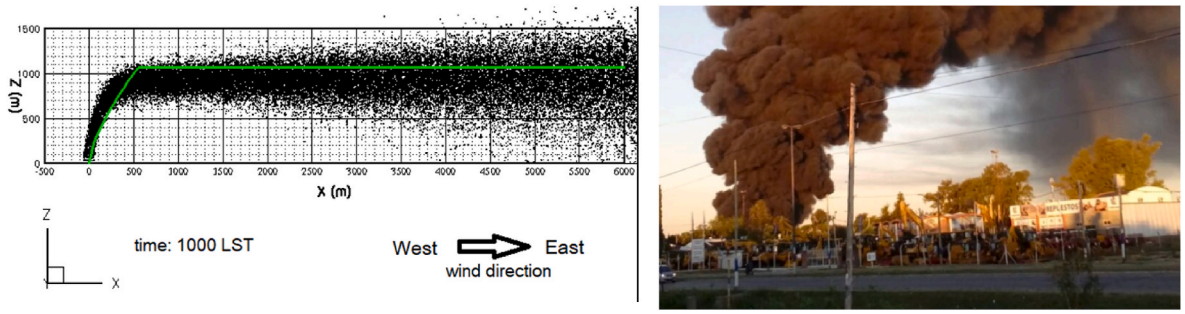

Fig. 8. Left: West-east vertical cross-section, seen from the south, of fluid particles distribution at 1000 LST. The green line represents the plume axis calculated with the Briggs algorithm. Right: Photograph of the fire taken at 1000 LST. (For interpretation of the references to color in this figure legend, the reader is referred to the Web version of this article.)

a vertically integrated view from above.

In the early morning, the NW wind predicted by the model moves the plume to the SE, after which the wind begins a rotation first to the SW and then to the S and the wind-driven plume continuously changes its spatial orientation, pointing North at 1300 LST. The wind direction changes shown by the model coincide with the observations of the meteorological stations in the region, as shown in Fig. 5.

Due to the changes of temperature and wind conditions during the simulation period, the modeled smoke plume begins to rise after 1200 LST such that the bottom of the plume exceeds 1200 m near the Mafissa plant. This accounts for the empty space near the source in the 1300 LST panel in Fig. 7, although due to the increased volume of the smoke plume it falls back further away from the source.

Fig. 7 compares the spatial layout of the modeled smoke plume with the visible smoke plume in the satellite image. The left panel of Fig. 7 shows the Sentinel-2 image of March 20, 2018 at 1058 LST in which the lateral limits have been drawn in dashed lines in order to facilitate appreciating the smoke plume layout. The right panel of Fig. 7 shows the smoke plume modeled at 1100 LST, with same dashed lines as the left panel to facilitate the comparison. Clearly, there is very good match between the position and spatial orientation of the modeled smoke plume at 1100 LST and the smoke plume as seen in the satellite image.

The left panel of Fig. 8 depicts a west-east vertical cross-section, as seen from the south, of the fluid particles distribution that simulates the smoke plume at 1000 LST, i.e. 3 h after the emission started, when the plume was oriented towards the east. The right panel of Fig. 8 shows the photography taken at same time. It can be seen that some particles have settled on the ground, indicating that the smoke reached the breathing level at some earlier time. The distance between the fire source and the place where the particles reached the ground is about 4 km. The green line in the left panel of Fig. 8 represents the plume axis calculated with the Briggs algorithm, which shows that the e plume rise simulated by the model is appropriate. The BLM model outputs at 1000 LST allow calculating the plume rise according to the Briggs algorithm with the following results: $\overline{U_3^{(t_0)}} = 4.18\, m\, s^{-1}$, $F_b = 96756.43\, m^4\, s^{-3}$, $\Delta z = 1000\, m$, $S_0 = 4.6\, m\, s^{-1}$, $T_a^{(t_0)} = 291.54\, K$, $\overline{T}_a = 290.03\, K$, $\Delta T_a = -3.01\, K$ and $stab = 2.286x10^{-4}\, s^{-2}$.

5. Conclusions

The availability of the high resolution Sentinel-2 satellite image with a visible smoke plume of a huge fire in the city of La Plata, Argentina, is used to verify the result of the simulation of the smoke plume with the fluid particle dispersion model LES-STO. The initial and boundary conditions necessary for running the model are provided by a boundary layer model forecast. Local meteorological observations are used to validate the wind and temperature forecast with good results. The modeled smoke plume is defined by the concentration of fluid particles that are continuously emitted at a constant rate from the location of the fire source. The emission of fluid particles begins 4 h before the verification time in order to allow the model to spin-up, since during this time interval the wind direction changed 90° and the wind speed increased. The spatial orientation and horizontal lateral extension of the modeled plume coincide with the smoke plume clearly visible in the satellite image. Also, the simulated over-elevation of the smoke plume matches the result of a well-known algorithm for the calculation of plume axis over-elevation. The conclusion of the study is that it is possible to use LES-STO with initial and boundary conditions provided by operational meteorological forecasts to make a diagnosis of those areas that could be affected by accidental emissions. The availability of an atmospheric dispersion forecast such as the one presented here, can assist local authorities in the adoption of appropriate mitigation measures, by having timely information about the areas that could be potentially affected by

harmful accidental emissions.

CRediT authorship contribution statement

Cesar Aguirre: Conceptualization, Methodology, Software, Review and Editing original draft. **Guillermo Berri:** Meteorological data, Initial and boundary conditions data, Writing – original draft, Reviewing and Editing. **Mariana Dezzutti:** Validation, of preliminary results. **Juan Martin Queirel:** Performance of model runs and verification of results. **Eliana Marcos:** Preparation of input files and boundary conditions model. **Carlos Sedano:** Software, preparation and control of model runs. **Guillermo Rondán:** Preparation of meteorological files.

Declaration of competing interest

The authors declare that they have no known competing financial interests or personal relationships that could have appeared to influence the work reported in this paper.

Acknowledgments

This work is supported by the Fund for Scientific and Technological Research (FONCYT), Argentina through PICT 2017-1670 research project, the National University of Entre Rios, Argentina, through PID-UNER 2242 research project, and the National University of La Plata, Argentina, through PID 2021-11/G176 research project and Program ProMeteo. The simulations were done using the Advanced Regional Prediction System (ARPS) developed by the Center for Analysis and Prediction of Storms, University of Oklahoma coupled to the stochastic one-particle model. The authors also acknowledge the fruitful comments and suggestions made by the anonymous reviewers that contributed to improving the quality of the paper.

Appendix A. Discrete solution of the fluid particle motion

The first line of equation (5) gives the position of the (ith) fluid particle, which is solved using a second order Runge–Kutta method (midpoint) as follows:

$$X_i^{(t+\Delta t)} = X_i^{(t)} + \left(U_i^{(t)} + U_i^{(t+\Delta t)}\right)\frac{\Delta t}{2} \tag{A.1}$$

The second line of equation (5) gives the fluid particle velocity in which the resolved scale by LES, $du_i^{\oplus}$, is calculated in fully three-dimensional curvilinear coordinates of ARPS code (Xue et al., 2000) using forward in time finite differences. The α_{ij} tensor is computed according to the hypothesis of statistically inhomogeneous isotropic turbulence, following Aguirre et al. (2006). The solution of second line of equation (5) requires calculating the sub-grid wind velocity of fluid particle $u_i^{\ominus(t+\Delta t)}$. Gardiner (1985) originally proposed that the sub-grid velocity of a fluid particle follows a Brownian motion, so that its initial value can be expressed as:

$$u_i^{\ominus(t_0)} = \sqrt{\frac{2}{3}k^{\ominus(t_0)}}\chi_i^{(t_0)}, \tag{A.2}$$

where $k^{\ominus(t_0)}$ is the sub-grid scale of turbulent kinetic energy computed by ARPS code following Deardorff (1980) and $\chi_i^{(t_0)}$ is a random variable with zero mean and variance equal to one. The superscript (t_0) indicates the initial time step of the simulation when the fluid particle is ejected from the source. The initial velocity of fluid particles of second line of equation (5) can be written as:

$$U_i^{(t_0)} = U_{3(i)}^{(t_0)} + u_i^{\oplus(t_0)} + u_i^{\ominus(t_0)}, \tag{A.3}$$

where $U_{3(i)}^{(t_0)}$ is the initial vertical velocity of the (ith) fluid particle due to thermal effects of the fire, calculated following equation (22). The sub-grid fluid particle velocity due to subgrid-scale wind turbulence, $u_i^{\ominus(t+\Delta t)}$, is calculated at each new time step as:

$$u_i^{\ominus(t+\Delta t)} = \alpha_{ij}u_j^{\ominus(t)}\Delta t + \sqrt{C_0\varepsilon}\delta_{ij}\,\Delta\eta_j^{(t)}, \tag{A.4}$$

where $\Delta\eta_j$ is the increment of a vector-valued Wiener process with zero mean and variance Δt:

$$\Delta\eta_j^{(t)} = \sqrt{\Delta t}\chi_j^{(t)}. \tag{A.5}$$

The right-hand side indicates that the variable has a variance Δt, as long as the variance of random variable $\chi_j^{(t)}$ is equal to one and its mean value equal to zero.

The random function allows obtaining a set random numbers *RAND* in the range [0, 1] with a continuous uniform distribution. In order to obtain a random variable with zero mean value and variance equal to one, the central limit theorem can be used:

$$\chi_j^{(t)} = \frac{<\xi^{(t)}> - m}{\sigma/\sqrt{N}}, \tag{A.6}$$

where $<\xi^{(t)}> = \frac{\sum_{k=1}^{N}[(\xi^{(t)})_k]}{N}$ is the mean of N values obtained of $\xi^{(t)} = RAND$ and σ is the standard deviation of ξ in the range [0, 1]. Michelot (1996) showed that if $N = 50$ it is possible to use the random function for obtaining a good approximation to a continuous uniform distribution function in the range [0, 1], in which case $\sigma = \sqrt{\frac{1-0}{12}} = \frac{\sqrt{3}}{6}$ and $m = 0.5$.

Appendix B. Discrete solution of the heat diffusion equation

Equation (8) can be written in a simplified form as:

$$T'_f = K\left(T_s - T_f\right) \tag{B.1}$$

where $T'_f = dT_f/dt$ is the time derivative of the fluid particle temperature and $K = C_{dif}/2\,t_t$.

Defining $T_s - T_f = -y$, its time derivative can be written as $T'_f = y'$ assuming that T_s is constant. Since the time step of calculations $\Delta t = 1\ s$, changes between time intervals are very small so that the assumption that $T'_s = 0$ is reasonable.

Equation (B.1), expressed as $y' = -K\,y$ is a first order ordinary differential equation whose solution is:

$$y^{(t)} = e^{-K\,t\,+\,\mathscr{C}}, \tag{B.2}$$

where $\mathscr{C}$ is an integration constant and superscript (t) indicates the time step. Similarly, at time step $(t+\Delta t)$ the discrete solution to (B.1) is:

$$y^{(t+\Delta t)} = e^{-K(t+\Delta t)+\mathscr{C}} \tag{B.3}$$

The ratio of (B.3) to (B.2) is:

$$y^{(t+\Delta t)} = y^{(t)}\ e^{-K\,\Delta t} \tag{B.4}$$

Recalling the assumption that T_s is constant and substituting $-y = T_s - T_f$, the solution to equation (9) is:

$$T_f^{(t+\Delta t)} - T_s^{(t)} = e^{-K\,\Delta t}\left(T_f^{(t)} - T_s^{(t)}\right) \tag{B.5}$$

References

Achtemeier, G.L., Goodrick, S.A., Liu, Y., Garcia-Menendez, F., Hu, Y., Odman, M.T., 2011. Modeling smoke plume-rise and dispersion from Southern United States prescribed burns with Daysmoke. Atmosphere 2, 358–388. https://doi.org/10.3390/atmos2030358, 2011.

Aguirre, C.A., Brizuela, A.B., 2016. Computational tools for the simulation of atmospheric pollution transport during a severe wind event in Argentina. In: Atmospheric Hazards - Case Studies in Modeling, Communication, and Societal Impacts, Chapter 6. INTECH Open Science, Open Mind, pp. 111–136. https://doi.org/10.5772/63552.

Aguirre, C.A., Brizuela, A.B., Vinkovic, I., Simoëns, S., 2006. A subgrid Lagrangian stochastic model for turbulent passive and reactive scalar dispersion. Int. J. Heat Fluid Flow. Elsevier Sci. 27 (4), 627–635. https://doi.org/10.1016/j.ijheatfluidflow.2006.02.011.

Aguirre, C.A., Berri, G.J., Brizuela, A.B., Orcellet, E.E., 2014a. External weather data assimilation to simulate wind and temperature fields in the region of Gualeguaychú, Argentina. J. Mech. Eng. Autom. 4, 887–899, 2014.

Aguirre, C.A., Aceñolaza, P.E., Brizuela, A.B. y Sedano C.G., 2014b. Simulación computacional de la dispersión de partículas sólidas en la atmósfera utilizando un modelo acoplado. Revista Científica de Mecánica Computacional. Santa Fe, Argentina XXXIII (52), 3431–3453.

Awad, C., Frangieh, N., Marcelli, T., Accary, G., Morvan, D., Meradji, S., Chatelon, F.J., Rossi, J.L., 2021. Numerical study of the moisture content threshold under prescribed burning conditions. Fire Saf. J. 122, 103324.

Berbery, E.H., Ciappesoni, H.C., Kalnay, E., 2008. The smoke episode in Buenos Aires, 15–20 April 2008. Geophys. Res. Lett. 35 (21).

Berri, G.J., Bertossa, G., 2018. Initializing a mesoscale boundary layer model with radiosonde observations. Boundary-Layer Meteorol. 166 (1), 137–151. https://doi.org/10.1007/s10546-017-0295-5.

Berri, G.J., Dezzutti, M., 2020. A sea breeze case study in the La Plata River region using local observations, satellite images and model simulations. Boundary-Layer Meteorol. 177 (1), 123–147. https://doi.org/10.1007/s10546-020-00548-3.

Berri, G.J., Sraibman, L., Tanco, R., Bertossa, G., 2010. Low-level wind field climatology over the La Plata River region obtained with a mesoscale atmospheric boundary layer model forced with local weather observations. J. Appl. Meteorol. Climatol. 49 (6), 1293–1305. https://doi.org/10.1175/2010JAMC2370.1.

Beyler, C.L., 2002. Fire hazard calculations for large open hydrocarbon fires. In: The SFPE Handbook of Fire Protection Engineering, third ed. Society of Fire Protection Engineering and National Fire Protection Association, Quincy, MA.

Bilyaz, S., Buffington, T., Ezekoye, O.A., 2021. The effect of fire location and the reverse stack on fire smoke transport in high-rise buildings. Fire Saf. J. 126, 103446.

Blanco, J.E., Berri, G.J., 2013. New indices for the spatial validation of plume forecasts with observations of smoke plumes from grassfires. Atmos. Environ. 67, 313–322.

Briggs, G.A., 1975. Plume rise predictions. In: Lectures on Air Pollution and Environmental Impact Analyses. American Meteorological Society, Boston, MA, USA, pp. 72–73, 1975.

Briggs, G.A., 1984. In: Randerson, D. (Ed.), Plume Rise and Buoyancy Effects. Atmospheric Science and Power Production. U.S. Dept. of Energy DOE/TIC27601, pp. 327–366 available from NTIS as DE84005177.

Cetegen, B.M., Zukoski, E.E., Kubota, T., 1984. Entrainment in the near and far field of fire plumes. Combust. Sci. Technol. 39, 305–331.

Cressman, G.P., 1959. An operational objective analysis system. Mon. Weather Rev. 87, 367–878.

Davies, H., 1983. Limitations of some common lateral boundary schemes used in regional NWP models. Mon. Weather Rev. 111, 1002–1012.

Deardorff, J.W., 1980. Stratocumulus-capped mixed layer derived from a three dimensional model. Boundary-Layer Meteorol. 18, 495–527.

Egorova, V.N., Trucchia, A., Pagnini, G., 2022. Fire-spotting generated fires. Part II: the role of flame geometry and slope. Appl. Math. Model. 104, 1–20.

Fackrell, J., Robins, A., 1982. Concentration fluctuation and fluxes in plumes from point sources in a turbulent boundary layers. J. Fluid Mech. 117, 1–26.

Gardiner, C.W., 1985. Handbook of Stochastic Methods, second ed. Springer-Verlag.

Germano, M., Piomelli, U., Moin, P., Cabot, W.H., 1991. A dynamic subgrid-scale eddy viscosity model. Physics of Fluids. A (3), 1760–1765.

Gicquel, L.Y.M., Givi, P., Jabri, F.A., Pope, S.B., 2002. Velocity filtered density function for large-eddy simulation of turbulent flows. American Institute of Physics Phys. Fluids 14 (3), 1196–1213.

Golubnichiy, A.A., Nedelina, D.O., 2015. Review and analysis of the modelling of the atmospheric air pollution for urban air basins. Journal "Naukovedenie 7 (5), 1–14. https://doi.org/10.15862/02TangVN515. http://naukovedenie.ru/PDF/02TangVN515.pdf (open access).

Gong, W., 1991. A wind tunnel study of turbulent dispersion over two – and three-dimensional gentle hills from upwind point sources in neutral flow. Boundary Layers Meteorology 54, 211–230.

Haworth, D.C., Pope, S.B., 1986. A generalized Langevin model for turbulent flow. Phys. Fluids 29 (2), 378–405.

Heskestad, G., 1983. Virtual origins of fire plumes. Fire Saf. J. 5, 109–114.

Heskestad, G., 1984. Engineering relations for fire plumes. Fire Saf. J. 7, 25–32.

Heskestad, G., 2016. Fire plumes, flame height and air entrainment, 978-1-4939-2565-0. In: The SFPE Handbook of Fire Protection Engineering book. Fifth Edition Volume I. Ed: Morgan J. Hurley. Springer New York Heidelberg, Dordrecht London, ISBN 978-1-4939-2564-3, pp. 396–428. https://doi.org/10.1007/978-1-4939-2565-0 (eBook).

Hsu, A.T., Chen, J.-Y., 1991. A continuous mixing model for p.d.f. simulation and its applications to combusting shear flow. Eighth Symposium on turbulent shear flow 22.4.1–22.4.5.

Jenkins, M.A., Clark, T., Coen, J., 2001. Coupling atmospheric and fire models. In: Johnson, E.A., Miyanishi, K. (Eds.), Forest Fires: Behavior and Ecological Effects. Academic Press, San Diego, CA, USA, pp. 258–301.

Liu, Y., Achtemeier, G.L., Goodrick, S., Jackson, B., Qu, J., 2011. Evaluation and improvement of smoke plume rise models. In: JFSP Research Project Reports U.S. Joint Fire Science Program. University of Nebraska, Lincoln U.S., pp. 1–19

Lyon, R.E., Hackett, S.M., Walters, R.N., 1998. Heats of combustion of high-temperature polymers. In: Technical Report Documentation N° DOT/FAA/AR-TN97/8. US Department of Transportation, Federal Aviation Administration. Springfield, Virginia, 22161, p. 18, 1998.

McCaffrey, B.J., 1979. Purely Buoyant-Diffusion Flames: Some Experimental Results, NBSIR79- 1910. National Bureau of Standards, Department of Commerce, Washington, D.C, 1979.

Michelot, C., 1996. Développement d'un Modèle Stochastique Lagrangien. Application à la Dispersion et à la Chimie de l'Atmosphère. Thèse de Doctorat. *Ecole Centrale de Lyon. France*, pp. 1–180.

Morton, B.R., 1959. Forced plumes. J. Fluid Mech. 5, 151–163.
Morton, B.R., Taylor, G.I., Turner, J.S., 1956. Turbulent gravitational convection from maintained and instantaneous sources. Proc. Roy. Soc. A 234, 1–23.
Orcellet, E.E., Berri, J.G., Aguirre, C.A., Müller, G.V., 2016. Atmospheric dispersion study of TRS compounds emitted from a pulp mill plant in coastal regions of the Uruguay River, South America. Aerosol and air quality research. Taiwan Assoc. Aerosol Res. 16 (6), 1473–1482. https://doi.org/10.4209/aaqr.2015.02.0112.
Perfil, 2018. Un gigantesco incendio devastó la fábrica textil más grande de La Plata. (20-03-2018. https://www.perfil.com/20-03-2018.html.
Pope, S.B., 1983. Consistent modeling of scalars in turbulent flows. Phys. Fluids. Am. Ins. Phys. 26 (2), 404–408.
Pope, S.B., 1985. PDF methods for turbulent reactive flow. Prog. Energy Combust. Sci. 11, 119–192.
Ratto, G., Berri, G.J., Maronna, R., 2014. On the application of hierarchical cluster analysis for synthesizing low-level wind fields obtained with a mesoscale boundary layer model. Meteorol. Appl. (3), 21. https://doi.org/10.1002/met.1396, 2014.
Sedano, C.G., Aguirre, C.A., Brizuela, A.B., 2019. Numerical simulation of spray ejection from a nozzle for herbicide application: comparison of drag coefficient expressions. Comput. Electron. Agric. 157, 136–145.
Sedano, C.G., Aguirre, C.A., Rondán, G.A., Brizuela, A.B., 2020. Numerical simulation of spray ejection from a nozzle for herbicide application: evaporation and Binary Collision Models. Comput. Electron. Agric. 175 https://doi.org/10.1016/j.compag.2020.105551.
Sraibman, L., Berri, G.J., 2009. Low level wind forecast over La Plata River region with a mesoscale boundary layer model forced by regional operational forecasts. Boundary-Layer Meteorol. 130 (3), 407–422. https://doi.org/10.1007/s10546-009-9350-1.
Stubbs, D.C., Humphreys, L.H., Goldman, A., Childtree, A.M., Kush, J.S., Scarborough, D. E., 2021. An experimental investigation into the wildland fire burning characteristics of loblolly pine needles. Fire Saf. J. 126, 103471.
Tagliaferri, F., Invernizzi, M., Capelli, L., 2022. A sensitivity analysis applied to SPRAY and CALPUFF models when simulating dispersion from industrial fires. Atmos. Pollut. Res. 13 https://doi.org/10.1016/j.apr.2021.101249.
Vinkovic, I., Aguirre, C.A., Ayrault, M., Simoëns, S., 2006. Large-eddy Simulation of the Dispersion of Solid Particles in a Turbulent Boundary Layer- Boundary-Layer Meteorology, 121, pp. 283–311.
Xue, M., Droegemeier, K., Wong, V., 2000. The advanced regional prediction system (ARPS). A multi-scale nonhydrostatic atmospheric simulation and prediction model. Part I: model dynamics and verification. Meteorol. Atmos. Phys. 75, 161–193.
Yih, C.S., 1952. Free Convection Due to a Point Source of Heat. Proceedings of the U.S. National Congress of Applied Mechanics, New York, pp. 941–947.
Zukoski, E.E., Cetegen, B.M., Kubota, T., 1984. Visible structure of buoyant diffusion flames. Twentieth Symposium (International) on Combustion. The Combustion Institute 361–366.